ASME Journal of Biomechanical Engineering
Online journal at:
https://asmedigitalcollection.asme.org/biomechanical

Yuankai Lu
Department of Ophthalmology,
University of Pittsburgh,
Pittsburgh, PA 15219
e-mail: YUL363@pitt.edu

Yi Hua
Department of Ophthalmology,
University of Pittsburgh,
Pittsburgh, PA 15219;
Department of Biomedical Engineering,
University of Mississippi,
Oxford, MS 38677;
Department of Mechanical Engineering,
University of Mississippi,
Oxford, MS 38677

Po-Yi Lee
Department of Ophthalmology,
University of Pittsburgh,
Pittsburgh, PA 15219;
Department of Bioengineering,
University of Pittsburgh,
Pittsburgh, PA 38677

Andrew Theophanous
Department of Bioengineering,
University of Pittsburgh,
Pittsburgh, PA 15261

Shaharoz Tahir
Department of Bioengineering,
University of Pittsburgh,
Pittsburgh, PA 15261

Qi Tian
Department of Bioengineering,
University of Pittsburgh,
Pittsburgh, PA 15261

Ian A. Sigal[1,2]
Department of Ophthalmology,
University of Pittsburgh,
Pittsburgh, PA 15219;
Department of Bioengineering,
University of Pittsburgh,
Pittsburgh, PA 15261
e-mail: ian@OcularBiomechanics.com

Lamina Cribrosa Hypoxia Sensitivity to Variations of Anatomy and Vascular Factors

Insufficient oxygenation in the lamina cribrosa (LC) may contribute to axonal damage and glaucomatous vision loss. To understand the range of susceptibilities to glaucoma, we aimed to identify key factors influencing LC oxygenation and examine if these factors vary with anatomical differences between eyes. We reconstructed three-dimensional, eye-specific LC vessel networks from histological sections of four healthy monkey eyes. For each network, we generated 125 models varying vessel radius, oxygen consumption rate, and arteriole perfusion pressure. Using hemodynamic and oxygen supply modeling, we predicted blood flow distribution and tissue oxygenation in the LC. ANOVA assessed the significance of each parameter. Our results showed that vessel radius had the greatest influence on LC oxygenation, followed by anatomical variations. Arteriole perfusion pressure and oxygen consumption rate were the third and fourth most influential factors, respectively. The LC regions are well perfused under baseline conditions. These findings highlight the importance of vessel radius and anatomical variation in LC oxygenation, providing insights into LC physiology and pathology. Pathologies affecting vessel radius may increase the risk of LC hypoxia, and anatomical variations could influence susceptibility. Conversely, increased oxygen consumption rates had minimal effects, suggesting that higher metabolic demands, such as those needed to maintain intracellular transport despite elevated intra-ocular pressure (IOP), have limited impact on LC oxygenation. [DOI: 10.1115/1.4068577]

Keywords: glaucoma, lamina cribrosa, vasculature, hemodynamics, oxygenation, blood flow

1 Introduction

Millions of people worldwide suffer from blindness or reduced vision due to glaucoma, a disease characterized by the degeneration of retinal ganglion cells and their axons [1,2]. In glaucoma, axonal damage is widely believed to initiate at the lamina cribrosa (LC) region within the optic nerve head (ONH) [3,4]; however, alternative hypotheses suggest that damage may begin at the

[1]Corresponding author.
[2]Present address: Laboratory of Ocular Biomechanics, Department of Ophthalmology, University of Pittsburgh, UPMC Mercy Pavilion, 1622 Locust Street, Rm. 7.382, Pittsburgh, PA 15219.
Manuscript received August 27, 2024; final manuscript received April 29, 2025; published online June 11, 2025. Assoc. Editor: Jolanda J. Wentzel.

neuroretinal rim [5] or within the brain [6]. The LC receives blood with nutrients and oxygen through a complex and dense vascular network that is intertwined with the collagen beams and the retinal ganglion cell axons [7–11]. Although the precise mechanisms of axon damage in LC remain unclear, one of the leading hypotheses posits that insufficient perfusion and oxygenation within the LC may contribute to cause the axonal damage [12–17].

The LC microcirculation could be influenced by various factors, including vascular network geometry, perfusion blood pressure, tissue metabolic demands, tissue deformations, autoregulation responses, and tissue remodeling mechanisms [8,18–20]. These factors could act independently or interact with each other, impacting both tissue perfusion and oxygenation, and thereby influencing physiological and pathological scenarios. Moreover, elevated intra-ocular pressure (IOP), one of the primary risk factors for glaucoma, could also contribute to this process. Elevated IOP can lead to deformation, compression, and distortion of the LC vasculature, compromising blood and oxygen supply to the LC region [14,19,21–23]. Our previous work also showed that LC oxygenation is more susceptible to systematic IOP-induced deformation than stochastic vasculature damage [24]. However, the critical threshold of IOP for glaucoma varies among patients, and many individuals with elevated IOP never suffer full vision loss due to glaucoma [25]. To address the variation among different eyes and identify the most influential factors, a systematic analysis involving multiple eyes and various potential risk factors affecting LC hemodynamics and oxygenation is necessary. Such systematic investigations are crucial for advancing our understanding of glaucoma pathophysiology and developing more effective diagnostic and therapeutic strategies.

Despite major advances of imaging techniques over the last several years, such as optical coherence tomography angiography (OCT-A) [26–29], ultrasound techniques [30], MRI-based techniques [31], and laser speckle flowgraphy [32], obtaining direct measurements of LC hemodynamics and oxygenation with adequate resolutions and depth penetration remains elusive. Therefore, alternative approaches, such as theoretical modeling and numerical simulations, have been employed to assess blood flow and oxygenation within the LC region [14,15,21,24,33,34]. Recently, we utilized experimentally derived reconstructed three-dimensional (3D) model of eye-specific LC vasculature and computational techniques for analyzing hemodynamics and oxygenation, and their influential factors [34]. We found that vessel radius, oxygen consumption rate, and arteriole perfusion pressure were the three most significant factors influencing LC oxygenation. However, the study was preliminary and based on a single eye anatomy. Eyes, however, vary in anatomy, and a result applicable to one eye is not necessarily exactly the same for another. Hence, it remains unclear whether the factor influences identified on our previous study generalize to other eyes.

Our goal in this study was to identify the most influential factors and address the impact of eye anatomy differences on LC oxygenation. To achieve our objective, four eye-specific 3D models of the LC vasculature were reconstructed based on histological sections. From this, numerical simulations were performed to evaluate LC hemodynamics and oxygenation. Specifically, we parameterized the vessel radius, oxygen consumption rate, and arteriole perfusion pressure to evaluate their impact on LC oxygen supply. We used a regularized grid to generate parameter combinations, allowing for the analysis of the independent and correlated effects of each parameter.

2 Methods

General procedure. First, we labeled, imaged, and reconstructed the eye-specific ONH vasculatures of four healthy monkeys as our baseline models, following the technique described elsewhere [35,36]. Based on the four baseline vascular network models, we then created 500 models by varying vessel radius, neural tissue oxygen consumption rate, and arteriole blood pressure (four eyes, five levels per parameter, three parameters: $4 \times 5^3 = 500$). Second, we performed hemodynamics and oxygenation simulations to evaluate the blood supply and from this the oxygen field within the ONHs. Third, we compared the fraction of hypoxic regions and the minimum oxygen tension within the LC across all models to determine the factor influences on LC hemodynamics and oxygenation. The steps are described in detail below.

2.1 Reconstruction of 3D Eye-Specific Lamina Cribrosa Vascular Network. All procedures were approved by the University of Pittsburgh's Institutional Animal Care and Use Committee, and followed both the guidelines set forth in the National Institutes of Health's Guide for the Care and Use of Laboratory Animals and the Association of Research in Vision and Ophthalmology statement for the use of animals in ophthalmic and vision research.

2.1.1 Vessel Labeling. We processed four healthy female rhesus macaque monkeys' heads for vessel labeling. The animals were raised under similar conditions. The ages of the monkeys at the time of sacrifice were 15, 16, 14, and 13 years for eyes 1, 2, 3, and 4, respectively. Within 2 h after sacrifice, we cannulated the anterior chamber of each eye to control IOP throughout the experiment. IOP was set to 5 mmHg to prevent hypotony or hypertension. Two polyimide microcatheters were inserted into the carotid arteries for labeling. Warm phosphate-buffered saline (PBS) was perfused to wash out intravascular blood first. A lipophilic carbocyanine dye, DiI, was then used to label the vessels in the eye. We perfused 100 ml DiI solution into each carotid artery, followed by a 100 ml 10% formalin perfusion to fixate the eye.

2.1.2 Histology and 3D Vasculature Reconstruction. The ONH and surrounding sclera were then isolated, cryoprotected, and sectioned [37]. Each section underwent imaging through fluorescence microscopy for vessel visualization and polarized light microscopy for collagen visualization [35,38]. 3D vasculature reconstruction involved importing and registering sequential these images in AVIZO software (version 9.1). Vessel segmentation aided by a Hessian filter, and vessels in the LC region were identified by the presence of collagen beams [35]. Our reconstructed vascular networks included the whole LC region and some of the prelaminar and retrolaminar regions (Fig. 1). This ensured that the 3D LC network was fully enclosed within the region reconstructed.

2.1.3 Vessel Diameter Setting. Although our reconstruction technique could be leveraged to obtain the vessel diameter information, we acknowledge that postmortem changes, tissue swelling, and pressure variations can alter vessel diameters from in vivo conditions. Autoregulation, particularly in the deep ONH and lamina cribrosa (LC), remains uncharacterized in vivo. Following previous studies of LC hemodynamics [14,15,24,33,34], we assumed that all vessels in the LC had the same diameter. A uniform capillary radius of 4 μm was selected based on prior measurements [40], as discussed in Ref. [34]. Further research, combining our technique with in vivo imaging, could improve our understanding of vessel diameters and autoregulation in the LC.

2.1.4 Vascular Reconstruction Validation. The postmortem dye perfusion process may encounter challenges, such as incomplete penetration into all vessel segments due to intravascular clotting or insufficient perfusate volume. To reduce clotting, we minimized the interval between animal death and perfusion and thoroughly washed the ONH with PBS. Our imaging revealed strong signals in retinal and choroidal vessels, indicating successful perfusion and sufficient labeling. Nevertheless, we acknowledge that vessel visualization and reconstruction could be impacted by uneven labeling, discontinuities, or leaks. Manual corrections, including "cleaning" and "bridging" segments, were performed to address these issues, though they may introduce artifacts and randomness [34,35]. To evaluate the reconstruction technique, two students independently reconstructed the same labeled eye, and their results were compared to assess the method's validity. Reconstruction 1 and reconstruction 2 represent the two independent reconstructions of the same eye. The

total vessel lengths for reconstruction 1 and reconstruction 2 were 547.68 mm and 528.68 mm, respectively, differing by only 3.3%. The average LC oxygen partial pressures were 55.56 mmHg and 54.85 mmHg, a difference of 1.3%.

Figure 2 illustrates the vessel geometry and oxygenation difference of reconstruction 1 and reconstruction 2, where the shared vasculature (yellow) included 9584 segments. Reconstruction 1 included 1334 unique segments, and reconstruction 2 included 859 unique segments. The shared vasculature accounts for approximately 90% of the total vessels in both models. The oxygenation differences were minimal, further demonstrating the high repeatability of the reconstruction process.

2.2 Hemodynamics and Oxygenations

2.2.1 Oxygen Diffusion in Tissue. We followed the approach described in Ref. [41] to perform the LC hemodynamics and oxygenation simulations. Oxygen transport within the oxygen-consuming neural tissues can be described by the reaction–diffusion equation [42]

$$D\alpha\Delta P_{O2} = M(P_{O2})$$

$$M(P_{O2}) = M_0 P_{O2}/(P_0 + P_{O2})$$

where D is the oxygen diffusion coefficient, α is the oxygen solubility coefficient, and P_{O2} is the tissue oxygen partial pressure. The oxygen consumption term $M(P_{O2})$ can be estimated by Michaelis–Menten enzyme kinetics [42], where M_0 represents oxygen demand and P_0 is the oxygen partial pressure at half-maximal consumption. In this study, M_0 was assumed to be uniform throughout the LC.

2.2.2 Oxygen Flux in Blood. Optic nerve head vascular network system was considered as a set of interconnected capillary elements. The capillary elements connect with each other at the bifurcation nodes. The blood flow within a capillary can be approximately by the Poiseuille's flow due to the low Reynolds number (<0.05) [43]

$$Q = \frac{\pi r^4}{8\mu L}\Delta P$$

where Q is the flow rate, r is the vessel radius, L is the vessel length, μ is the blood viscosity, and ΔP is the pressure drop along the vessel. The blood viscosity μ was described as a function of vessel radius

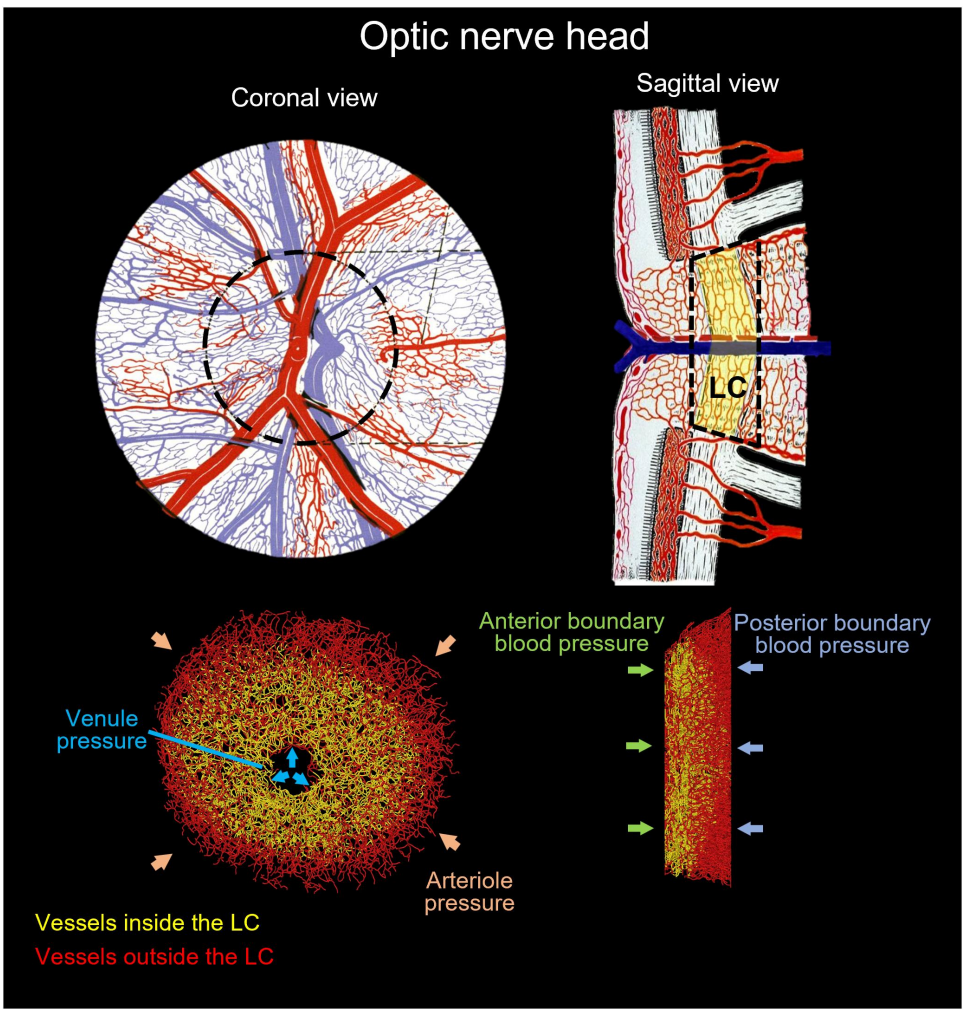

Fig. 1 (Top) Diagram of the ONH adapted from Ref. [39]. Our model represents the vessels within the scleral canal, included the whole LC region, and some of the prelaminar and retrolaminar regions. Black dashed lines represent the model boundaries, and yellow area represents the LC region. (Bottom) An example eye-specific vessel network. To improve flow boundary conditions, the region reconstructed extended beyond the LC. Vessels within the LC are shown colored in yellow. Vessels reconstructed but outside the LC are shown in red. The network is labeled to illustrate the blood pressure boundary condition settings. Four blood pressure conditions were assigned at the peripheral, central, anterior, and posterior boundaries of the model. See the main text for the rationale and details on how these pressures were assigned. (Color version online.)

and hematocrit (i.e., the volume fraction of red blood cells). The behavior of red blood cell flow in small vessels is complex and beyond the scope of this study, but readers are encouraged to read the papers by Pries and Secomb [44] and by Ebrahimi and Bagchi [45]. A detailed description of the effective viscosity is provided in the Appendix. For a baseline vessel diameter of 8 μm, the effective viscosity was approximately 7.65×10^{-3} mPa·s in this work.

2.2.3 Blood Pressure Boundary Conditions. The model boundaries were divided into four regions for assigning the blood pressure conditions that drive the blood flow throughout the vascular network (Fig. 1).

At the periphery: An arteriole pressure of 50 mmHg was set as baseline to represent blood inflow from the circle of Zinn–Haller [14,15].

At the center: A venule pressure of 15 mmHg was set as baseline to represent blood drainage through the central retinal vein [14,15,46].

Many previous studies of LC hemodynamics assumed no flow through the anterior and posterior LC boundaries, either explicitly or by assuming no vessel interconnections [15,47]. Our reconstructions show a large number of interconnections [35,48], and therefore we knew that we had to develop a new approach. We reasoned that the capillaries should remain open under normal conditions. This, in turn, required blood pressure to exceed the surrounding tissue pressure. Thus, for each boundary, we estimated the "worst-case" blood pressure based on the tissue pressure levels, which then differed for the anterior and posterior boundaries.

Anterior boundary: Prelaminar tissues are highly compliant, with minimal pressure drop, so tissue pressure was set equal to IOP (15 mmHg). Based on experimental [49] and numerical studies [50], a blood pressure of 20 mmHg was assigned for the anterior boundary, considering a 5 mmHg fluctuation due to the cardiac cycle.

Posterior boundary: The tissue pressure behind the LC, sometimes referred to as the retrolaminar tissue pressure (RLTP), is related to, but not identical to, cerebrospinal fluid pressure (CSFP). Based on Morgan et al. [49], RLTP can be approximated as $0.82 \times \text{CSFP} + 2.9$ mmHg. Assuming a CSFP of 10 mmHg [51,52], the estimated RLTP is 11 mmHg. The average posterior boundary blood pressure was set at 16 mmHg to prevent capillary collapse, considering a 5 mmHg cardiac cycle fluctuation.

Human retinal vein branches, with diameters ranging from 33.3 to 155.4 μm, exhibit blood flow velocities of 19.3 mm/s [53]. The mouse central retinal artery, ophthalmic artery, and long posterior ciliary artery have velocities of 20–30 mm/s [54], while human central retinal arteries exhibit velocities of 15–35 mm/s [55]. The 15 mm/s was considered to be characteristic of arterial flow and thus unphysiological for capillaries; this corresponds to a threshold of 45 nl/min in our baseline condition.

The oxygen flux in blood vessels satisfies

$$f(P_b) = Q(\alpha_{\text{eff}} P_b + H_D C_0 S(P_b))$$

where Q is the flow rate, α_{eff} is the effective solubility of oxygen in plasma, H_D is the hematocrit, C_0 is the concentration of hemoglobin-bound oxygen in a fully saturated red blood cell, P_b is the blood oxygen partial pressure (mmHg), and $S(P_b)$ is the oxygen–hemoglobin saturation, determined by the empirical oxygen–hemoglobin dissociation curve.

2.2.4 Oxygen Exchange on Vessel Walls. Conservation of oxygen along each vessel segment implied that

$$\frac{df(P_b)}{ds} = -q(s)$$

where s is arc-length parameter along the vessel, and $q(s)$ is the total oxygen flux through the blood vessel wall per unit vessel length.

At the interface between blood vessel and tissue, the diffusive oxygen flux across the vessel wall must be consistent with the surrounding tissue oxygenation, implying that

$$q(s) = -D\alpha \int_0^{2\pi} \frac{\partial P_{O2}}{\partial r} R d\theta$$

where r is the radial distance from the vessel centerline, R is the vessel radius, and the integral is around the circumference, denoted by angle θ. Therefore, the oxygen flux can be evaluated from the average gradient of P_{O2} on the vessel wall.

As reported before [41], we used a fast and efficient method to simulate the convective and diffusive oxygen transport in the complex ONH vascular networks. The method employs an implicit finite difference scheme with the multigrid algorithm to compute the tissue oxygen field, while blood oxygenation is modeled as a system

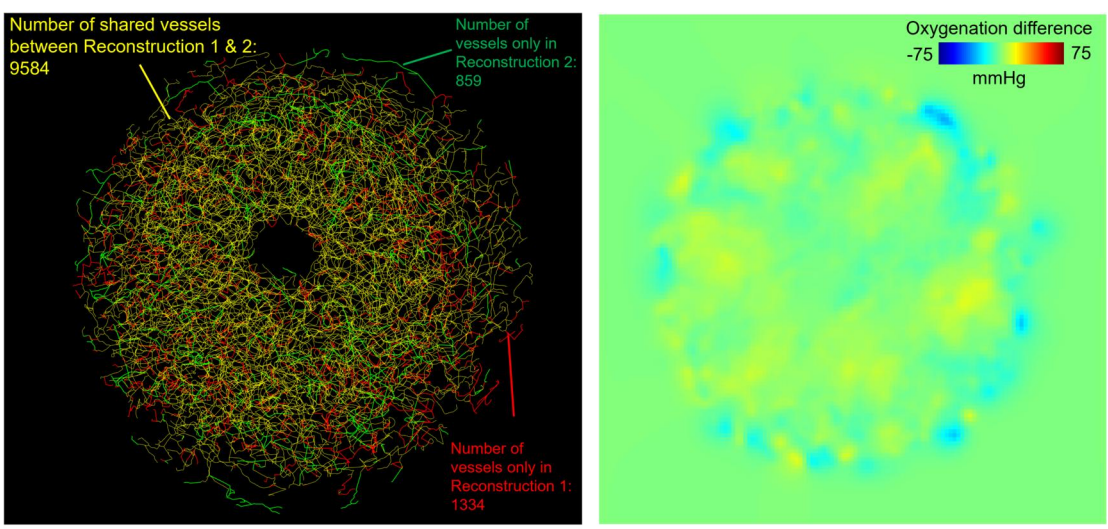

(*a*) (*b*)

Fig. 2 Repeatability of vascular reconstruction. Two independent reconstructions of the same labeled eye showed high geometric and oxygenation consistency. (*a*) Over 90% of vessels were shared between the reconstructions. (*b*) Oxygenation differences were minimal, with an average oxygen partial pressure difference of 0.71 mmHg. (Color version online.)

Table 1 Parameters used in hemodynamic and oxygenation simulations

Constant parameters	Value	References
Oxygen diffusion coefficient, $D\alpha$	6×10^{-10} $mlO_2/cm/s/mmHg$	[42]
Effective oxygen solubility, α_{eff}	3.1×10^{-5} $mlO_2/ml/mmHg$	[42]
Oxygenation at half-maximal consumption, P_0	10.5 mmHg	[42]
Maximal RBC oxygen concentration C_0	0.5 mlO_2/ml	[42]
Venule pressure	15 mmHg	[34]
Anterior blood pressure	20 mmHg	[34]
Posterior blood pressure	16 mmHg	[34]
Effective viscosity for 4 μm radius vessel	7.65×10^{-3} mPa·s	[44]
Inlet blood oxygenation	75 mmHg	[56]
Parametric factors		
Vessel radius	4 μm	[34]
Arteriole pressure	50 mmHg	[34]
Consumption rate, M_0	5×10^{-4} $mlO_2/ml/s$	[34]

of ordinary differential equations along the vessels. Oxygen exchange at the vessel wall is incorporated into the tissue oxygen discretization using a numerical delta distribution function. A physics-based iterative approach ensures convergence and accuracy of the nonlinear system. We used frequency for both blood flow and oxygenation analyses. For blood flow, frequency represents the fraction of capillary segments. For oxygenation, frequency represents the fraction of neural tissue points under the corresponding tissue oxygenation. All parameters are listed in Table 1.

2.3 Parametric Analysis. We performed a parametric analysis based on the variation of three parameters: vessel radius, neural tissue oxygen consumption rate, and arteriole pressures. These parameters were selected because they had the strongest influences on LC hemodynamics and oxygenation in our previous study [34]. Baseline values of the parameters were established from the literature, as shown in Table 1 and discussed in detail [34]. To provide a systematic and unbiased parametric analysis, these were all varied ±20% of the baseline (80–120%). Five parameter levels were selected: 80% (low), 90%, 100% (baseline), 110%, and 120% (high), resulting in a total of $5 \times 5 \times 5 = 125$ models for each eye. We repeated the same parametric analysis for all four eyes, resulting in a total of 500 models.

As outcome measures, we used the minimal oxygen tension in the LC and the tissue volume fraction of the hypoxia region [57–59]. For minimal oxygen tension, the 10th percentile was used as the definition of the minimal value to reduce the influence of very small regions that could be artifactual [34].

Tissue hypoxia, characterized by reduced tissue oxygenation, is generally a consequence of structurally and functionally disturbed microcirculation [60,61]. We discussed this issue in length in a previous publication [24].

Hypoxia can be categorized into:

(1) Normoxia: Normal cellular activity and metabolism.
(2) Mild hypoxia: Physiological responses. If sustained chronically, it may contribute to neural tissue damage.
(3) Severe hypoxia: Tissue necrosis, irreversible damage.

This study focuses on parametric evaluation for chronic pathologies, such as glaucoma. To simplify the analysis, we adopted mild hypoxia as the threshold, as it reflects conditions that may contribute to chronic injury without immediate tissue necrosis.

The hypoxia threshold for ONH is unknown and could vary from species and individuals. We conducted a literature survey for normoxia/hypoxia, with the findings summarized below. The 8 mmHg (∼1% oxygen) has been consistently used as a threshold for severe hypoxia in neural tissues [62–64]. Tissue normoxia, however, varies widely, from 20 mmHg to 50 mmHg, and is difficult to measure under in vivo ONH conditions [60,64–66]. Considering the hypoxia-sensitive neural cells in the LC region, we analyzed precedents set in existing literature; in the normal ONH and cerebral cortex [61,63,66,67]. We settled on a threshold of 38 mmHg (∼5% oxygen) for tissue normoxia, as used in Ref. [58]. We selected a threshold in the upper end of values reported in the literature, reasoning that it may be more relevant for chronic conditions. Selecting a lower threshold would decrease the estimates of hypoxic region fraction.

2.4 Statistical Analysis. We utilized ANOVA to assess the rank and statistical significance of all parameters. Specifically, we used the percentage of the total sum of squares corrected by the mean as a metric to represent the contribution of each parameter and interaction [17]. The results among different eyes were analyzed collectively, where the eye itself was considered as a categorial factor in ANOVA to account for individual variations in our models. Further details regarding the statistical analysis can be found in our previous parametric work [34].

3 Results

The baseline hemodynamics and oxygenation of the four networks are shown in Fig. 3. Although the eyes differed in anatomy, their hemodynamic and oxygenation exhibited similar characteristics. The flow rate and oxygenation were high at the periphery and low at center. This pattern is consistent with the blood supply for LC, where blood perfusion is from the periphery, draining through the central retinal vein. A 3D oxygenation map of eye 1 is shown in Fig. 4. Flow rates in the vessel network vary significantly in scale. The average flow rate across the four ONHs at baseline is approximately 3.31 nl/min, with the highest flow reaching 104 nl/min. The flow rate distribution for eye 1 is shown in Fig. 5, indicating that nearly all ONH flow rates remain within physiological ranges. Detailed illustrations of flow and oxygen pattern are shown in Fig. 6 and Video 1 (see Supplemental Materials on the ASME Digital Collection).

Table 2 summarizes the measurements for the four eyes. Our analysis showed that the average distance to the nearest vessel was similar for eyes 1 and 2 and was larger for eyes 3 and 4. However, other parameters, including segment number, branch point number, and tortuosity, did not follow this grouping pattern. Interestingly, the overall region volumes were smallest for eyes 3 and 4. This suggests that differences in distance parameter may contribute to the observed grouping of oxygenation patterns. Nevertheless, LC

Table 2 Geometric parameters for the four eye vasculatures

	Segment number	Branch point number	Region volume (mm^3)	Total length (mm)	Average distance to nearest vessel (μm)	Average tortuosity
Eye 1	12,966	9089	1.456	646.6	53.478	1.129
Eye 2	10,918	8886	1.304	528.7	52.545	1.114
Eye 3	12,012	9436	1.298	547.8	56.026	1.115
Eye 4	10,700	8151	1.169	628.3	61.621	1.270

The distance was defined as the mean distance from each LC tissue point to its closest vessel. The tortuosity was calculated as the ratio of the vessel segment path length to its end-to-end distance.

oxygenation is influenced by multiple factors, and a larger sample size is necessary to further identify the relationship between vascular geometry and ONH oxygenation.

Figure 7 illustrates oxygenation distribution under various radii, consumption rates, and arteriole pressures for eye 1. We selected three levels—low (80%), baseline (100%), and high (120%)—to show the impact of each parameter on LC oxygenation. Notably, changes in vessel radius caused the largest changes in LC oxygenation distribution, while variations in other parameters had comparatively smaller effects.

Boxplots of the impact of each factor on the 10th percentile oxygenation and the fraction of hypoxic regions across all eyes are presented in Fig. 8. Vessel radius exhibited the strongest positive relationship with the 10th percentile oxygenation and the strongest negative relationship with the fraction of hypoxic regions, consistent with the results shown in Fig. 7. The statistical significance of each parameter was evaluated via ANOVA (see Fig. 9). The most influential factors were vessel radius, arteriole pressure, and oxygen consumption rate. There were weak interactions between these influential factors. Specifically, the interactions between radius and pressure are illustrated in Fig. 10.

4 Discussion

Our goal was to identify the most influential factors on LC oxygenation, including the impact of eye to eye anatomical variations. Specifically, we used four eye-specific 3D LC vasculature models and parameterized the vessel radius, oxygen consumption rate, and arteriole perfusion pressure to evaluate their impact on LC oxygen levels. The four most influential factors on LC oxygenation were, from most to least influential: vessel radius, eye anatomy, arteriole perfusion pressure, and oxygen consumption rate. Our models also showed that the LC was well irrigated at baseline IOP. Below, we discuss the findings in more detail as well as the limitations and other considerations to keep in mind when interpreting them.

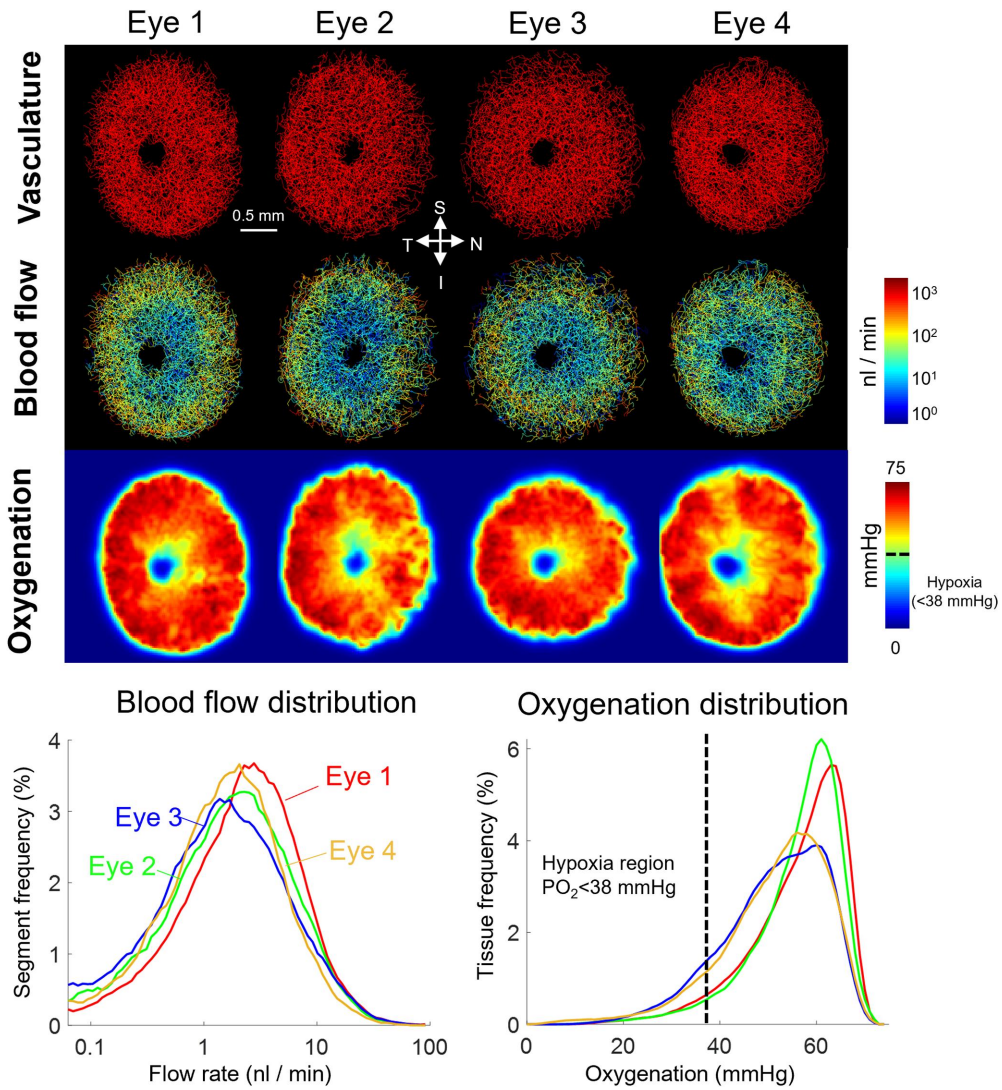

Fig. 3 Vascular geometry, baseline hemodynamics, and baseline oxygenation of four eyes. Top: Vascular geometry and maps of blood flow and oxygenation. Bottom: Distributions of blood flow and oxygenation in the LC region. Blood flow and oxygenation exhibited similar features and tendencies across all eyes. Higher flow rates and oxygenation occurred at the periphery of the LC region, and lower flow rates and oxygenation were observed at the center. Interestingly, the distribution curves of blood flow and oxygenation showed different patterns. Blood flow exhibited significant variation across the entire LC, ranging from 1 to 1000 nl/min, while the LC was consistently well-provided with oxygen. Oxygen tensions remain consistently high throughout most of the LC region, with minimal regions experiencing hypoxic conditions.

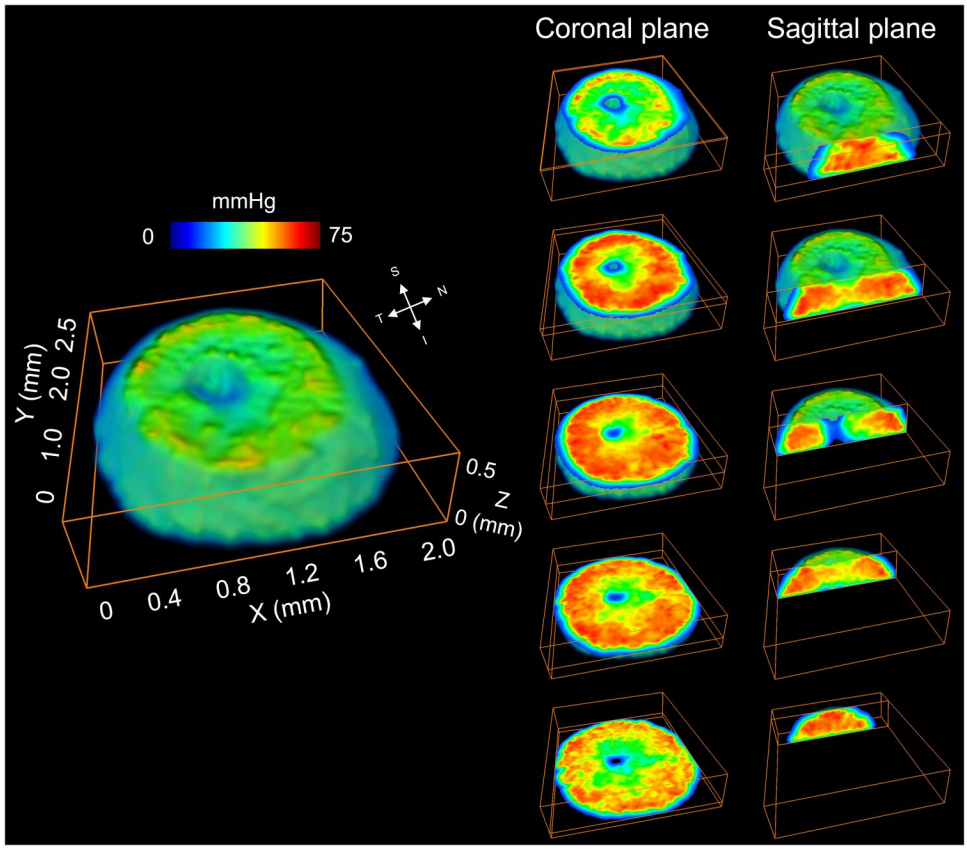

Fig. 4 Three-dimensional oxygenation map for eye 1 ONH. Five sections were selected for visualization in the coronal and sagittal planes. In the coronal sections, the peripheral region generally exhibits higher oxygenation levels compared to the central region. However, regions near the model boundary, such as the superficial plane or the extreme peripheral rim, also show reduced oxygenation levels. While the entire ONH model is shown, our analysis is focused on the LC region.

4.1 Vessel Radius Was the Most Influential Factor on the Lamina Cribrosa Oxygenation. Our models predicted that the vessel radius has the strongest contribution to LC oxygenation, both for the 10th percentile oxygenation and hypoxia region fraction. This can be understood as follows: Vessel radius plays a crucial role in determining the flow resistance of each vessel segment, as evidenced by the well-known quartic power in Poiseuille's flow formula. By precisely controlling luminal radius through vessel wall contraction and dilation, this sensitivity can be leveraged by vascular systems to regulate blood and oxygen supply efficiently. There are, however, some scenarios in which the high sensitivity to vessel radius could prove problematic to LC perfusion. For example, IOP-induced deformations can distort the LC tissues, altering the geometry of the vessels within, altering radius. Substantial

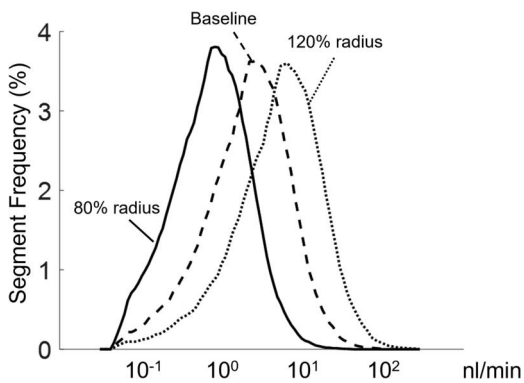

Fig. 5 Flow rate distribution for eye 1 under different radii. As expected, the flow rates increase as the radii were larger. The average flow rates were 1.06, 3.31, and 8.23 nl/min when the radius was adjusted to 80%, 100%, and 120% of the baseline value, respectively. Very few vessels have ocular arterial-level flows (>45 nl/min), with 0.1% for the baseline case and 0.7% for the 120% case.

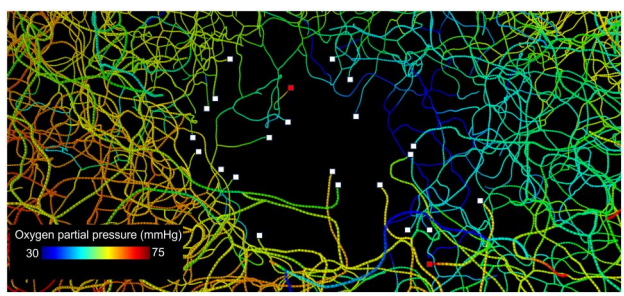

Fig. 6 A screenshot of the video illustrating red blood cell transport in the blood vessels. The region shown is a close-up of the drainage at the central retinal vessels. Colors represent the blood oxygen saturation. The dots along each vessel represent the red blood cells. White and red squares represent blood flow outlets and inlets, respectively. The vessel ends in the center of the LC serve as flow outlets, according to the boundary conditions of flow drainage through the center retinal vein. Vessel ends that are not draining are because they end at the model anterior/posterior boundary (see Fig. 1), and thus flow can be to/from the LC. Notably, the blood oxygen saturation exhibits an asymmetric pattern at the center, with lower oxygenation observed on the right side (nasal side). (Color version online.)

experimental evidence supports the idea that blood perfusion in the ONH decreases and vessel radius reduces with elevated IOP [15,33,68–70]. Thus, our model predictions are consistent with the literature. Given the complexity of the LC mechanics and vascular network, predicting the effects of IOP-related deformations on LC oxygenation is not trivial. Elsewhere, we have presented a combined experimental–computational analysis using models similar to those in this work [71]. We found that moderately elevated IOP can cause sufficient distortions to the LC vasculature to alter LC hemodynamics and lead to mild hypoxia in a substantial part of the LC. More extreme IOP elevations can lead to severe hypoxia that is likely to cause more immediate damage to the LC neural tissues.

4.2 Eye Anatomy Variations Had the Second Strongest Influence on the Lamina Cribrosa Oxygenation. Eye anatomy variations refer to the differences in oxygenation between eyes. This means that for vascular networks modeled with exactly the same parameters and differing only on the vascular network, the hemodynamics and oxygenation were substantially and significantly different. As shown in Sec. 3, the four models formed two groups. See, for example, the plot of LC oxygenation in Fig. 3. The models of eyes 1 and 2 show similar curves, distinct from the curves of eyes 2 and 4. It is important for readers to recall that the response curves will change as other parameters vary, however, the ANOVA results indicate that the changes in the curves will be similar for all the eyes since there were no significant interactions between eye anatomy and other parameters. This means that eyes differ in hemodynamics and oxygenation, but that their sensitivity to changes in other parameters is the same. Thus, while it is still not clear why some eyes, or their vascular networks, behave differently, there is a common similar sensitivity. Some eyes may be more susceptible to low oxygenation than others, but it seems to be that this is not because of a higher sensitivity to the parameters. Our recent work investigated the IOP effect on LC oxygenation across different eyes [71]. Different eyes anatomy led to different LC oxygenation. However, the changes of LC oxygenation due to IOP-induced deformation were similar for all eyes, which also suggest the common sensitivity.

Previously, we conducted a study similar to this one, using a 3D eye-specific model of the LC vasculature to evaluate how hemodynamics and oxygenation were affected by varying several parameters [34]. We found that vessel radius, oxygen consumption rate, and arteriole perfusion pressure were the three most significant factors influencing LC oxygenation. In that study, however, we used only one vascular network and therefore were unable to evaluate the effects of eye anatomy. This is why it was crucial to conduct the study described in this paper.

Other studies have looked at variations in LC hemodynamics resulting from differences or changes in anatomy. Most of these

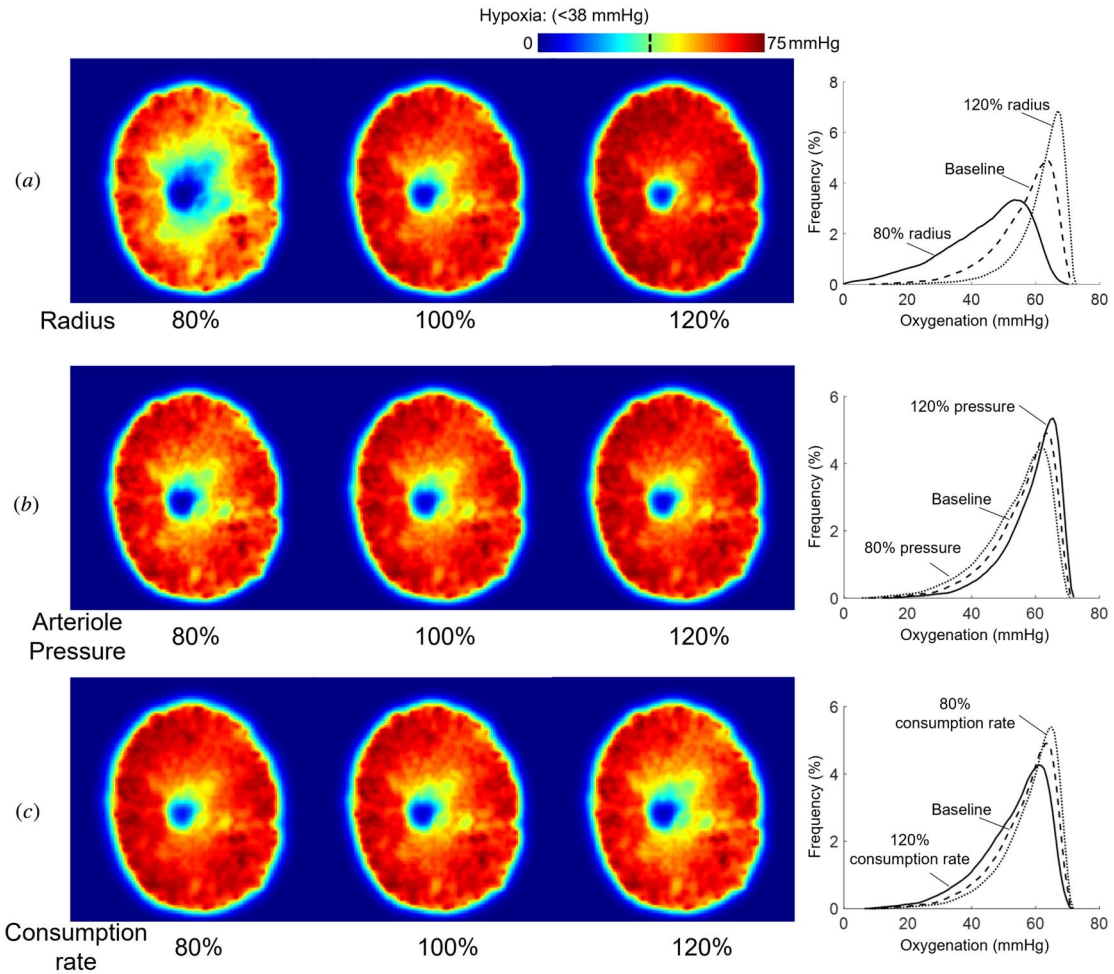

Fig. 7 Oxygenation distribution across various radii, consumption rates, and arteriole pressures for eye 1. (*a*) Oxygenation at different radii. (*b*) Oxygenation at different arteriole pressures. (*c*) Oxygenation at different consumption rates. Three levels—low (80%), baseline (100%), and high (120%)—were selected to illustrate the impact of each parameter. Radius demonstrated the strongest positive influence on oxygenation, while consumption rate and arteriole pressure had minor effects. Most hypoxia regions were observed near the center of the LC across all parametric scenarios.

studies have considered the LC as a generic model, varying parameters such as the LC size, depth, and curvature [14,15,33,47]. These studies found that structural parameters, such as cup depth and LC stiffness, had the most significant influence on LC oxygenation during IOP elevation. This was followed by perfusion pressure, while other structural parameters, such as anisotropy and pole size, had a weaker impact on LC oxygenation compared to perfusion pressure. The ranking of influence strength was analyzed using similar techniques as presented in Fig. 9. Overall, LC structural parameters, or eye anatomy, play a crucial role in influencing LC oxygenation, which is consistent with our findings in this work.

The simplified generic models have several important strengths, as we have discussed elsewhere [72], but there are also disadvantages. Generic models can potentially miss core details of

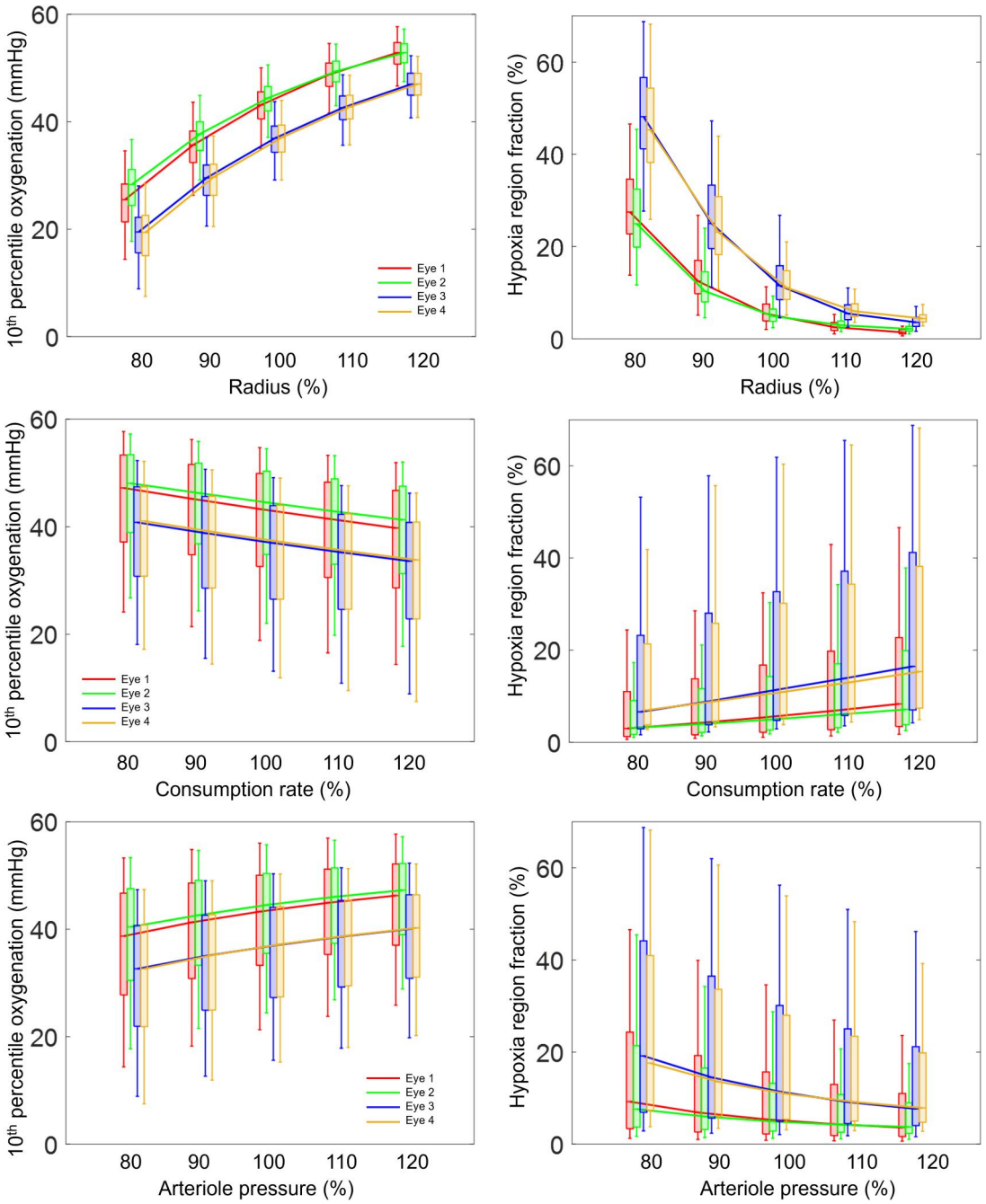

Fig. 8 Boxplots showing the factor influences on the 10th percentile oxygenation and hypoxia region fraction in the lamina cribrosa across all eyes. The top and bottom edges of each box are the upper and lower quartiles (25th and 75th percentiles), while the line inside of each box is the sample median (50th percentiles), respectively. The end of the whiskers shows the minimum and maximum. To aid visualization, we added lines connecting the median values. Vessel radius shows the strongest positive relationship with the 10th percentile oxygenation and the strongest negative relationship with the hypoxia region fraction. The variation observed among different eyes exceeds the oxygenation difference between scenarios with 80% consumption rate/arteriole pressure and those with 120% consumption rate/arteriole pressure. Interestingly, eyes 1 and 2 exhibited similar LC oxygenation across all parametric cases, while eyes 3 and 4 also showed similar patterns to each other but differed from eyes 1 and 2. The changes in LC oxygenation in response to the parameters, or in other words, the sensitivity to parameters, were consistent across all eyes.

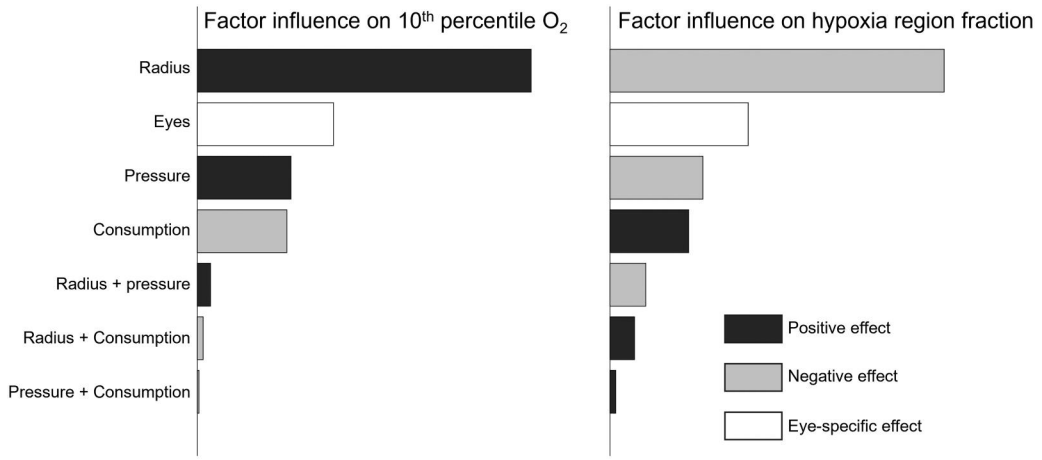

Fig. 9 Bar chart showing the influence of factors and interactions on the 10th percentile oxygenation and hypoxia region fraction in the LC, as determined by ANOVA. The factors are listed in descending order of their influence. The vessel radius was strongest influence factor, followed by the eye, arteriole pressure, and consumption rate. Interactions between the parameters show minor contributions to the LC oxygenation.

the architecture of a specimen. Also, it is possible that the parameter space considered by the generic models does not represent the actual variability of eyes, not just in terms of the parameters and their ranges, but their distributions. If this is the case, the sensitivities may be inaccurate. Further, it is possible that generic models fail to account properly for model complexity and variability and thus miss important conditions. This is where the use of eye-specific models reveals an important strength that we leveraged in this work. Eye anatomy, however, remains a discrete parameter. Elsewhere, we have shown techniques that potentially could be adapted to parameterize eye-specific models [34].

4.3 Arteriole Perfusion Pressure and Oxygen Consumption Rate Ranked Third and Fourth Most Influential Factors on Lamina Cribrosa Oxygenation. Arteriole perfusion pressure and oxygen consumption rate ranked as the third and fourth influential factors on LC oxygenation. The LC oxygenation was positively associated with the arteriole perfusion pressure and negatively associated with the oxygen consumption rate. LC oxygenation reflects the balance between supply and consumption. Increased perfusion pressure would drive more blood flow across the LC and bring more oxygen to neural tissues. Conversely, a higher oxygen consumption rate would consume more oxygen in LC, potentially leading to hypoxia under insufficient supply. Perfusion pressure came from the cardiovascular circulation and was affected by the upstream vascular systems and some blood flow regulation mechanism. Cardiovascular dysfunctions, such as hypo/hypertension, were found to be linked to glaucoma development [73–76]. It is worth noting that the hypo/hypertension will also induce the remodeling of vascular structures, such as systemic vasoconstriction (vessel radius reduction), capillary rarefaction, which may also alter the LC hemodynamics and oxygenations [77–79]. The oxygen consumption rate in LC varied based on the amount, type, and activity of various cells in neural tissues, including axons, astrocytes, and other cells, and could even change during the glaucoma development [59,63].

From a perspective of physiological mechanisms and biological functions, the perfusion pressure and consumption rate should directly affect the LC oxygenation, which aligns with our expectations and findings. Interestingly, they contribute less than the eye anatomy variations.

4.4 The Lamina Cribrosa Was Well Irrigated at Baseline. All the eyes were well irrigated under baseline conditions, with less than 15% of the LC volume suffering low enough oxygenation to be at risk of hypoxia. This is consistent with the idea

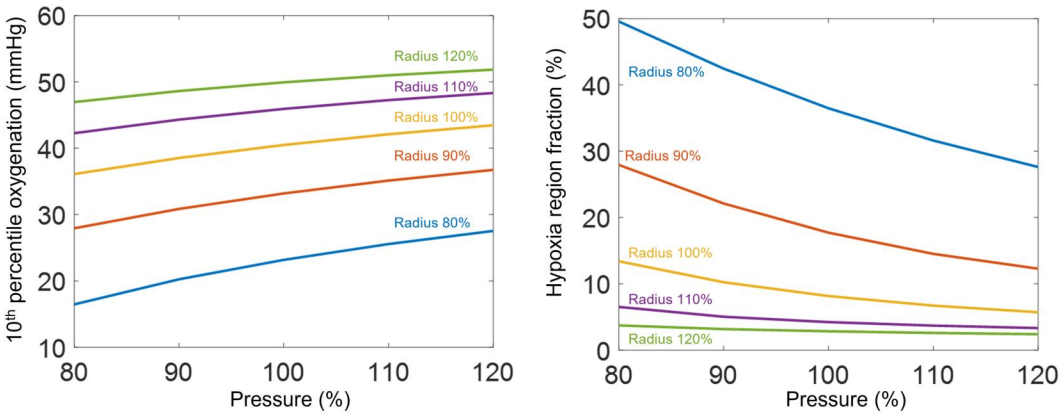

Fig. 10 Interactions between vessel radius and arteriole pressure on LC oxygenation. Regarding the 10th percentile oxygenation, the curves for different pressures were nearly parallel, suggesting a weak interaction between the radius and pressure parameters. For hypoxia region fraction, the influence of the pressure was stronger when the radius was low. An illustration of flow rate variations as a function of radius and pressure is provided in Fig. 11.

that healthy individuals have low risk of LC hypoxia. The result also agrees with our previous work on the robustness of the LC oxygenation [24].

To the best of our knowledge, this is the first study to conduct parametric analysis based on multiple 3D eye-specific LC models while accounting for eye anatomy. We combined the experimental-based reconstructed LC vasculature with highly accurate and efficient numerical simulation techniques to provide a high-resolution estimation of LC hemodynamics and oxygenation. Our reconstruction technique enables the creation of multiple LC vascular networks from histological sections of healthy monkeys, offering high-resolution and accurate structural detail. Utilizing a fast algorithm for hemodynamic and oxygenation simulations, we conducted a systematic parametric analysis across multiple eyes.

4.5 Limitations. It is important to acknowledge the limitations of this study so that readers can consider them when interpreting our findings. The first limitation is that we used computational modeling. While our techniques have been tested and verified, much better experimental data are required to consider the predictions from our models confirmed and validated. The LC is extremely complex, and there are still too many aspects that are not fully understood. Unfortunately, at this time, the experimental tools and techniques necessary to gather the data necessary do not exist. As discussed before, the challenges in spatial and temporal resolution and in signal penetration are not yet overcome. There are promising tools in the horizon, like visible light OCT that may enable measuring blood oxygenation [28] and super-resolution ultrasound that may allow measuring of blood flow with high resolution and deep into the ONH [54].

While this study expanded on our previous parametric analysis of LC hemodynamics and oxygenation by including several eye-specific models, another limitation is that using only four models is insufficient to fully capture the variability observed in human or monkey eyes. Future studies with a larger number of eye models, particularly including human eyes, are essential to better understand this variability.

Although we reconstructed the 3D eye-specific LC vasculature model from experimental images, we recognize that there were gaps between our reconstructed vasculature model and the in vivo LC vascular network. A salient one is that we set the vessel radius in LC as a uniform value. Currently, there are no studies offering detailed distributions of vessel radius in the LC, and the use of a uniform radius has been common in previous LC hemodynamic studies. Our reconstruction technique was based on ex vivo histological sections. The difference in the internal environment (e.g., absence of blood pressure, interstitial fluid pressure, and IOP) results in the different vessel radius from the in vivo case. Since our analysis indicates that the vessel radius was the strongest influential factor for LC oxygenation, it is important to consider the limitation of our uniform radius assumption and the potential effect due to the nonuniform radius distribution. Further research, potentially with a more advanced reconstruction technique coupled with in vivo imaging, could help provide detailed information on in vivo LC vessel radius and estimate the effect of the radius distribution.

Another limitation is that our work only considers the static status of LC hemodynamics and oxygenation. All the parameters in our model were assumed to be time-invariant and independent. However, in vivo blood/oxygen supply involves several regulation mechanisms to meet the changing demand of organisms. For instance, short-term blood flow autoregulation has been identified as a significant factor in hemodynamics and oxygenation for eye [18,80]. Long-term vessel remodeling in the LC has also been reported in the development of glaucoma [2,8]. Although the precise regulation and remodeling in LC remain unknown, we acknowledge that they could alter the LC blood and oxygen supply [10,18,20,80–82]. Future research should incorporate the dynamic aspects of the LC blood and oxygen supply, which might contribute to the development of pathology, such as glaucoma.

It is important to note that the LC and ONH in vivo are not static. Tissue distortions, for example, due to changes in IOP or gaze, can deform the vessels, affecting hemodynamics and potentially oxygenation. We recognize that such distortions can have a major impact and have thus explored them in a dedicated paper [83]. Specifically, using experimentally derived IOP-related distortions measured using optical coherence tomography and digital volume correlation, we found that moderately elevated IOP can cause LC vessel distortions that reduce oxygenation and can even lead to mild hypoxia in a substantial part of the LC. For extreme IOP elevations, severe hypoxia was predicted [83]. We have also used ultrasound techniques to explore the reductions on LC oxygenation resulting from IOP effects directly on the ONH and indirectly through the posterior ciliary arteries [84].

In summary, we used four reconstructed eye-specific 3D LC vasculature and parameterized the vessel radius, oxygen consumption rate, and arteriole perfusion pressure in our hemodynamic models to evaluate their impact on LC oxygen supply. Our model predicted that the vessel radius and eye variation had the most significant influence on the LC oxygen supply. Situations that alter the radius, such as IOP-induced deformation, may contribute to compromised LC oxygenation. But different individuals could also exhibit different susceptibility to those pathological scenarios due to their anatomy differences.

Funding Data

- National Institutes of Health R01-EY023966, R01-EY031708, R01-HD083383, P30-EY008098, and T32-EY017271 (Bethesda, MD) (Funder ID: 10.13039/100000053).
- The Eye and Ear Foundation (Pittsburgh, PA) (Funder ID: 10.13039/100001607).
- Research to Prevent Blindness (Stein innovation award to Sigal IA and unrestricted grant to UPMC ophthalmology; Funder ID: 10.13039/100001818).
- BrightFocus Foundation (Funder ID: 10.13039/100006312).

Data Availability Statement

The datasets generated and supporting the findings of this article are obtainable from the corresponding author upon reasonable request.

Appendix

A.1 Effective Viscosity. The effective viscosity μ within the blood vessel accounts for the Fåhræus–Lindqvist effect, which describes the dependence of blood viscosity on vessel radius and hematocrit.

In our model, we used the same rheological parameter settings used in Ref. [44] to compute effective blood viscosity in vivo. These settings are supported by experimental data from Ref. [85]. The effective viscosity μ was calculated using the following formula:

$$\mu = \left(1 + \left(\mu^*_{0.45} - 1\right) \cdot \frac{(1 - H_D)^C - 1}{(1 - 0.45)^C - 1} \cdot \frac{r^4}{(r - 0.55)^4}\right) \cdot \mu_{\text{plasma}}$$

$$C = \left(0.8 + \exp(-0.15r)\right) \cdot \left(-1 + \frac{1}{1 + 4 \cdot 10^{-8} * r^{12}}\right) + \frac{1}{1 + 4 \cdot 10^{-8} * r^{12}}$$

$$\mu^*_{0.45} = 6 \cdot \exp(-0.017r) + 3.2 - 2.44 \cdot \exp\left(-0.094r^{0.645}\right)$$

Here, the hematocrit H_D was set as 0.45, and plasma viscosity μ_{plasma} was set as 1.0466 mPa·s.

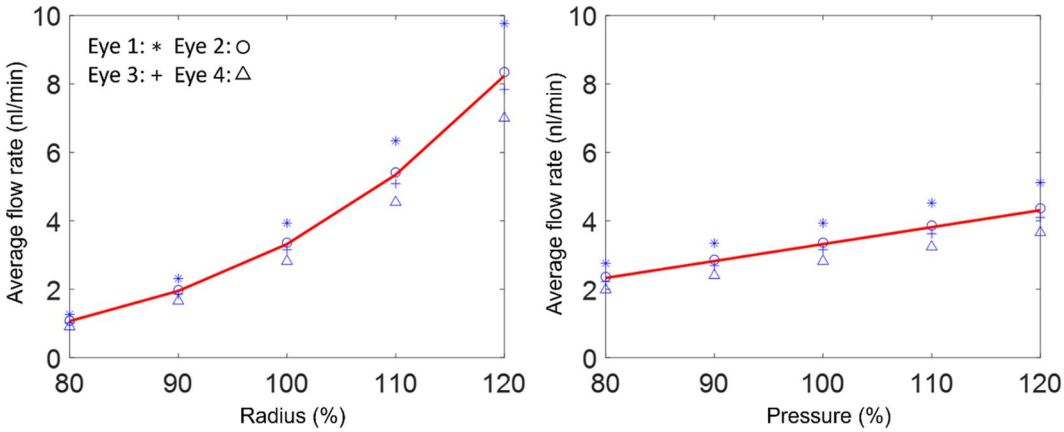

Fig. 11 Average flow rate change as a function of radius (left) and pressure (right). The flow rate changes slightly exceed the fourth power of the radius variation due to viscosity dependence. Flow rate changes are slightly less than the ratio of pressure difference change, as the pressure parameter only accounts for peripheral pressure, while anterior/posterior pressure remains unchanged in this analysis.

For a baseline vessel diameter of 8 μm, the effective viscosity was approximately 7.65×10^{-3} mPa·s.

A.2 Flow Rate Across Different Vessel Radii and Pressures. Figure 11 illustrates flow rate changes as a function of radius and pressure.

- The flow rate change slightly exceeds the fourth power of radius change, due to the fourth order relationship in Poiseuille's flow and the dependence of effective viscosity on vessel diameter.
- The flow rate change is slightly less than the ratio of pressure difference change, as the pressure parameter in this analysis only considers peripheral pressure, while anterior/posterior pressure remains unchanged in this parametric study.

References

[1] Quigley, H., and Anderson, D. R., 1976, "The Dynamics and Location of Axonal Transport Blockade by Acute Intraocular Pressure Elevation in Primate Optic Nerve," Invest. Ophthalmol. Visual Sci., **15**(8), pp. 606–616.

[2] Quigley, H. A., Nickells, R. W., Kerrigan, L. A., Pease, M. E., Thibault, D. J., and Zack, D. J., 1995, "Retinal Ganglion Cell Death in Experimental Glaucoma and After Axotomy Occurs by Apoptosis," Invest. Ophthalmol. Visual Sci., **36**(5), pp. 774–786.

[3] Howell, G. R., Libby, R. T., Jakobs, T. C., Smith, R. S., Phalan, F. C., Barter, J. W., Barbay, J. M., et al., 2007, "Axons of Retinal Ganglion Cells Are Insulted in the Optic Nerve Early in DBA/2J Glaucoma," J. Cell Biol., **179**(7), pp. 1523–1537.

[4] Quigley, H., 2011, "Glaucoma," Lancet, **377**(9774), pp. 1367–1377.

[5] Fortune, B., Reynaud, J., Hardin, C., Wang, L., Sigal, I. A., and Burgoyne, C. F., 2016, "Experimental Glaucoma Causes Optic Nerve Head Neural Rim Tissue Compression: A Potentially Important Mechanism of Axon Injury," Invest. Ophthalmol. Visual Sci., **57**(10), pp. 4403–4411.

[6] Kasi, A., Faiq, M. A., and Chan, K. C., 2019, "In Vivo Imaging of Structural, Metabolic and Functional Brain Changes in Glaucoma," Neural Regener. Res., **14**(3), pp. 446–449.

[7] Brazile, B. L., Yang, B., Waxman, S., Lam, P., Voorhees, A. P., Hua, Y., Loewen, R. T., et al., 2020, "Lamina Cribrosa Capillaries Straighten as Intraocular Pressure Increases," Invest. Ophthalmol. Visual Sci., **61**(12), p. 2.

[8] Hayreh, S., 1996, "The Optic Nerve Head Circulation in Health and Disease," Ophthalmic Lit., **2**(49), p. 111.

[9] Levitzky, M., and Henkind, P., 1969, "Angioarchitecture of the Optic Nerve: II. Lamina Cribrosa," Am. J. Ophthalmol., **68**(6), pp. 986–996.

[10] Mackenzie, P. J., and Cioffi, G. A., 2008, "Vascular Anatomy of the Optic Nerve Head," Can. J. Ophthalmol., **43**(3), pp. 308–312.

[11] Sugiyama, K., Bacon, D., Morrison, J., and Van Buskirk, E., 1992, "Optic Nerve Head Microvasculature of the Rabbit Eye," Invest. Ophthalmol. Visual Sci., **33**(7), pp. 2251–2261.

[12] Hamasaki, D., and Fujino, T., 1967, "Effect of Intraocular Pressure on Ocular Vessels: Filling With India Ink," Arch. Ophthalmol., **78**(3), pp. 369–379.

[13] Burgoyne, C. F., Downs, J. C., Bellezza, A. J., Suh, J.-K. F., and Hart, R. T., 2005, "The Optic Nerve Head as a Biomechanical Structure: A New Paradigm for Understanding the Role of IOP-Related Stress and Strain in the Pathophysiology of Glaucomatous Optic Nerve Head Damage," Prog. Retinal Eye Res., **24**(1), pp. 39–73.

[14] Chuangsuwanich, T., Birgersson, K. E., Thiery, A., Thakku, S. G., Leo, H. L., and Girard, M. J., 2016, "Factors Influencing Lamina Cribrosa Microcapillary Hemodynamics and Oxygen Concentrations," Invest. Ophthalmol. Visual Sci., **57**(14), pp. 6167–6179.

[15] Chuangsuwanich, T., Hung, P. T., Wang, X., Liang, L. H., Schmetterer, L., Boote, C., and Girard, M. J. A., 2020, "Morphometric, Hemodynamic, and Biomechanical Factors Influencing Blood Flow and Oxygen Concentration in the Human Lamina Cribrosa," Invest. Ophthalmol. Visual Sci., **61**(4), p. 3.

[16] Sigal, I. A., and Grimm, J. L., 2012, "A Few Good Responses: Which Mechanical Effects of IOP on the ONH to Study?," Invest. Ophthalmol. Visual Sci., **53**(7), pp. 4270–4278.

[17] Sigal, I. A., 2009, "Interactions Between Geometry and Mechanical Properties on the Optic Nerve Head," Invest. Ophthalmol. Visual Sci., **50**(6), pp. 2785–2795.

[18] Wang, L., Burgoyne, C. F., Cull, G., Thompson, S., and Fortune, B., 2014, "Static Blood Flow Autoregulation in the Optic Nerve Head in Normal and Experimental Glaucoma," Invest. Ophthalmol. Visual Sci., **55**(2), pp. 873–880.

[19] Pitha, I., Du, L., Nguyen, T., and Quigley, H., 2024, "IOP and Glaucoma Damage: The Essential Role of Optic Nerve Head and Retinal Mechanosensors," Prog. Retinal Eye Res., **99**, p. 101232.

[20] Hayreh, S. S., 2001, "Blood Flow in the Optic Nerve Head and Factors That May Influence It," Prog. Retinal Eye Res., **20**(5), pp. 595–624.

[21] Carichino, L., Guidoboni, G., Arieli, Y., Siesky, B. A., and Harris, A., 2012, "Effect of Lamina Cribrosa Deformation on the Hemodynamics of the Central Retinal Artery: A Mathematical Model," Invest. Ophthalmol. Visual Sci., **53**(14), p. 2836.

[22] Fechtner, R. D., and Weinreb, R. N., 1994, "Mechanisms of Optic Nerve Damage in Primary Open Angle Glaucoma," Surv. Ophthalmol., **39**(1), pp. 23–42.

[23] Quigley, H. A., McKinnon, S. J., Zack, D. J., Pease, M. E., Kerrigan–Baumrind, L. A., Kerrigan, D. F., and Mitchell, R. S., 2000, "Retrograde Axonal Transport of BDNF in Retinal Ganglion Cells is Blocked by Acute IOP Elevation in Rats," Invest. Ophthalmol. Visual Sci., **41**(11), pp. 3460–3466.

[24] Lu, Y., Hua, Y., Wang, B., Zhong, F., Theophanous, A., Tahir, S., Lee, P.-Y., and Sigal, I. A., 2024, "The Robust Lamina Cribrosa Vasculature: Perfusion and Oxygenation Under Elevated Intraocular Pressure," Invest. Ophthalmol. Visual Sci., **65**(5), p. 1.

[25] Racette, L., Wilson, M. R., Zangwill, L. M., Weinreb, R. N., and Sample, P. A., 2003, "Primary Open-Angle Glaucoma in Blacks: A Review," Surv. Ophthalmol., **48**(3), pp. 295–313.

[26] Mari, J. M., Strouthidis, N. G., Park, S. C., and Girard, M. J., 2013, "Enhancement of Lamina Cribrosa Visibility in Optical Coherence Tomography Images Using Adaptive Compensation," Invest. Ophthalmol. Visual Sci., **54**(3), pp. 2238–2247.

[27] Numa, S., Akagi, T., Uji, A., Suda, K., Nakanishi, H., Kameda, T., Ikeda, H. O., and Tsujikawa, A., 2018, "Visualization of the Lamina Cribrosa Microvasculature in Normal and Glaucomatous Eyes: A Swept-Source Optical Coherence Tomography Angiography Study," J. Glaucoma, **27**(11), pp. 1032–1035.

[28] Pi, S., Hormel, T. T., Wei, X., Cepurna, W., Wang, B., Morrison, J. C., and Jia, Y., 2020, "Retinal Capillary Oximetry With Visible Light Optical Coherence Tomography," Proc. Natl. Acad. Sci., **117**(21), pp. 11658–11666.

[29] Rao, H. L., Pradhan, Z. S., Weinreb, R. N., Riyazuddin, M., Dasari, S., Venugopal, J. P., Puttaiah, N. K., et al., 2017, "A Comparison of the Diagnostic Ability of Vessel Density and Structural Measurements of Optical Coherence Tomography in Primary Open Angle Glaucoma," PLoS One, **12**(3), p. e0173930.

[30] Qian, X., Kang, H., Li, R., Lu, G., Du, Z., Shung, K. K., Humayun, M. S., and Zhou, Q., 2020, "In Vivo Visualization of Eye Vasculature Using Super-Resolution Ultrasound Microvessel Imaging," IEEE Trans. Biomed. Eng., **67**(10), pp. 2870–2880.

[31] Li, Y., Cheng, H., and Duong, T. Q., 2008, "Blood-Flow Magnetic Resonance Imaging of the Retina," Neuroimage, **39**(4), pp. 1744–1751.

[32] Sugiyama, T., Araie, M., Riva, C. E., Schmetterer, L., and Orgul, S., 2010, "Use of Laser Speckle Flowgraphy in Ocular Blood Flow Research," Acta Ophthalmol., **88**(7), pp. 723–729.
[33] Causin, P., Guidoboni, G., Harris, A., Prada, D., Sacco, R., and Terragni, S., 2014, "A Poroelastic Model for the Perfusion of the Lamina Cribrosa in the Optic Nerve Head," Math. Biosci., **257**, pp. 33–41.
[34] Hua, Y., Lu, Y., Walker, J., Lee, P.-Y., Tian, Q., McDonald, H., Pallares, P., et al., 2022, "Eye-Specific 3D Modeling of Factors Influencing Oxygen Concentration in the Lamina Cribrosa," Exp. Eye Res., **220**, p. 109105.
[35] Lee, P.-Y., Hua, Y., Brazile, B. L., Yang, B., Wang, L., and Sigal, I. A., 2022, "A Workflow for Three-Dimensional Reconstruction and Quantification of the Monkey Optic Nerve Head Vascular Network," ASME J. Biomech. Eng., **144**(6), p. 061006.
[36] Waxman, S., Brazile, B. L., Yang, B., Lee, P.-Y., Hua, Y., Gogola, A. L., Lam, P., et al., 2022, "Lamina Cribrosa Vessel and Collagen Beam Networks Are Distinct," Exp. Eye Res., **215**, p. 108916.
[37] Tran, H., Jan, N.-J., Hu, D., Voorhees, A., Schuman, J. S., Smith, M. A., Wollstein, G., and Sigal, I. A., 2017, "Formalin Fixation and Cryosectioning Cause Only Minimal Changes in Shape or Size of Ocular Tissues," Sci. Rep., **7**(1), p. 12065.
[38] Jan, N.-J., Grimm, J. L., Tran, H., Lathrop, K. L., Wollstein, G., Bilonick, R. A., Ishikawa, H., Kagemann, L., Schuman, J. S., and Sigal, I. A., 2015, "Polarization Microscopy for Characterizing Fiber Orientation of Ocular Tissues," Biomed. Opt. Express, **6**(12), pp. 4705–4718.
[39] Hayreh, S. S., 1969, "Blood Supply of the Optic Nerve Head and Its Role in Optic Atrophy, Glaucoma, and Oedema of the Optic Disc," Br. J. Ophthalmol., **53**(11), pp. 721–748.
[40] An, D., Pulford, R., Morgan, W. H., Yu, D.-Y., and Balaratnasingam, C., 2021, "Associations Between Capillary Diameter, Capillary Density, and Microaneurysms in Diabetic Retinopathy: A High-Resolution Confocal Microscopy Study," Transl. Vis. Sci. Technol., **10**(2), p. 6.
[41] Lu, Y., Hu, D., and Ying, W., 2021, "A Fast Numerical Method for Oxygen Supply in Tissue With Complex Blood Vessel Network," PLoS One, **16**(2), p. e0247641.
[42] Secomb, T. W., Hsu, R., Park, E. Y., and Dewhirst, M. W., 2004, "Green's Function Methods for Analysis of Oxygen Delivery to Tissue by Microvascular Networks," Ann. Biomed. Eng., **32**(11), pp. 1519–1529.
[43] Pries, A. R., Secomb, T., Gessner, T., Sperandio, M., Gross, J., and Gaehtgens, P., 1994, "Resistance to Blood Flow in Microvessels In Vivo," Circ. Res., **75**(5), pp. 904–915.
[44] Pries, A. R., and Secomb, T. W., 2008, "Blood Flow in Microvascular Networks," *Microcirculation, Academic Press*, MA.
[45] Ebrahimi, S., and Bagchi, P., 2022, "A Computational Study of Red Blood Cell Deformability Effect on Hemodynamic Alteration in Capillary Vessel Networks," Scientific Reports, **12**(1), p. 4304.
[46] Mozaffarieh, M., Bärtschi, M., Henrich, P., Schoetzau, A., and Flammer, J., 2014, "Retinal Venous Pressure in the Non-Affected Eye of Patients With Retinal Vein Occlusions," Graefe's Arch. Clin. Exp. Ophthalmol., **252**(10), pp. 1569–1571.
[47] Causin, P., Guidoboni, G., Malgaroli, F., Sacco, R., and Harris, A., 2016, "Blood Flow Mechanics and Oxygen Transport and Delivery in the Retinal Microcirculation: Multiscale Mathematical Modeling and Numerical Simulation," Biomech. Model. Mechanobiol., **15**(3), pp. 525–542.
[48] Sigal, I. A., Lee, P.-Y., Quinn, M., Waxman, S., Voorhees, A. P., Yang, B., Jakobs, T. C., Rizzo, J., Fortune, B., and Hua, Y., 2022, "The Lamina Cribrosa Vascular Network is Heavily Interconnected With That of Adjacent Regions, Not Just the Periphery, Likely Improving Perfusion Resilience," Invest. Ophthalmol. Visual Sci., **63**(7), pp. 4031–A0416.
[49] Morgan, W. H., Yu, D.-Y., Alder, V. A., Cringle, S. J., Cooper, R. L., House, P. H., and Constable, I. J., 1998, "The Correlation Between Cerebrospinal Fluid Pressure and Retrolaminar Tissue Pressure," Invest. Ophthalmol. Visual Sci., **39**(8), pp. 1419–1428.
[50] Roberts, M. D., Liang, Y., Sigal, I. A., Grimm, J., Reynaud, J., Bellezza, A., Burgoyne, C. F., and Downs, J. C., 2010, "Correlation Between Local Stress and Strain and Lamina Cribrosa Connective Tissue Volume Fraction in Normal Monkey Eyes," Invest. Ophthalmol. Visual Sci., **51**(1), pp. 295–307.
[51] Feola, A. J., Myers, J. G., Raykin, J., Mulugeta, L., Nelson, E. S., Samuels, B. C., and Ethier, C. R., 2016, "Finite Element Modeling of Factors Influencing Optic Nerve Head Deformation Due to Intracranial Pressure," Invest. Ophthalmol. Visual Sci., **57**(4), pp. 1901–1911.
[52] Hua, Y., Voorhees, A. P., and Sigal, I. A., 2018, "Cerebrospinal Fluid Pressure: Revisiting Factors Influencing Optic Nerve Head Biomechanics," Invest. Ophthalmol. Visual Sci., **59**(1), pp. 154–165.
[53] Wang, Y., Lu, A., Gil-Flamer, J., Tan, O., Izatt, J. A., and Huang, D., 2009, "Measurement of Total Blood Flow in the Normal Human Retina Using Doppler Fourier-Domain Optical Coherence Tomography," Br. J. Ophthalmol., **93**(5), pp. 634–637.
[54] Ul Banna, H., Mitchell, B., Chen, S., and Palko, J., 2023, "Super-Resolution Ultrasound Localization Microscopy Using High-Frequency Ultrasound to Measure Ocular Perfusion Velocity in the Rat Eye," Bioengineering, **10**(6), p. 689.
[55] Guidoboni, G., Harris, A., Cassani, S., Arciero, J., Siesky, B., Amireskandari, A., Tobe, L., Egan, P., Januleviciene, I., and Park, J., 2014, "Intraocular Pressure, Blood Pressure, and Retinal Blood Flow Autoregulation: A Mathematical Model to Clarify Their Relationship and Clinical Relevance," Invest. Ophthalmol. Visual Sci., **55**(7), pp. 4105–4118.
[56] Chu, Y.-C., Chen, C.-Z., Lee, C.-H., Chen, C.-W., Chang, H.-Y., and Hsiue, T.-R., 2003, "Prediction of Arterial Blood Gas Values From Venous Blood Gas Values in Patients With Acute Respiratory Failure Receiving Mechanical Ventilation," J. Formosan Med. Assoc., **102**(8), pp. 539–543.
[57] Davies, A. L., Desai, R. A., Bloomfield, P. S., McIntosh, P. R., Chapple, K. J., Linington, C., Fairless, R., et al., 2013, "Neurological Deficits Caused by Tissue Hypoxia in Neuroinflammatory Disease," Ann. Neurol., **74**(6), pp. 815–825.
[58] McKeown, S., 2014, "Defining Normoxia, Physoxia and Hypoxia in Tumours—Implications for Treatment Response," Br. J. Radiol., **87**(1035), p. 20130676.
[59] Ortiz-Prado, E., Natah, S., Srinivasan, S., and Dunn, J. F., 2010, "A Method for Measuring Brain Partial Pressure of Oxygen in Unanesthetized Unrestrained Subjects: The Effect of Acute and Chronic Hypoxia on Brain Tissue PO2," J. Neurosci. Methods, **193**(2), pp. 217–225.
[60] Leach, R., and Treacher, D., 1998, "Oxygen transport2. Tissue Hypoxia," Bmj, **317**(7169), pp. 1370–1373.
[61] Ortiz-Prado, E., Dunn, J. F., Vasconez, J., Castillo, D., and Viscor, G., 2019, "Partial Pressure of Oxygen in the Human Body: A General Review," Am. J. Blood Res., **9**(1), pp. 1–14.
[62] Erecińska, M., and Silver, I. A., 2001, "Tissue Oxygen Tension and Brain Sensitivity to Hypoxia," Respir. Physiol., **128**(3), pp. 263–276.
[63] Beach, J., Ning, J., and Khoobehi, B., 2007, "Oxygen Saturation in Optic Nerve Head Structures by Hyperspectral Image Analysis," Curr. Eye Res., **32**(2), pp. 161–170.
[64] De Filippis, L., and Delia, D., 2011, "Hypoxia in the Regulation of Neural Stem Cells," Cell. Mol. Life Sci., **68**(17), pp. 2831–2844.
[65] Hockel, M., and Vaupel, P., 2001, "Tumor Hypoxia: Definitions and Current Clinical, Biologic, and Molecular Aspects," J. Natl. Cancer Inst., **93**(4), pp. 266–276.
[66] Carreau, A., Hafny-Rahbi, B. E., Matejuk, A., Grillon, C., and Kieda, C., 2011, "Why is the Partial Oxygen Pressure of Human Tissues a Crucial Parameter? Small Molecules and Hypoxia," J. Cell. Mol. Med., **15**(6), pp. 1239–1253.
[67] Ferrez, P., Chamot, S., Petrig, B., Pournaras, C., and Riva, C., 2004, "Effect of Visual Stimulation on Blood Oxygenation in the Optic Nerve Head of Miniature Pigs: A Pilot Study," Klin. Monatsbl. Augenheilkund., **221**(5), pp. 364–366.
[68] Boltz, A., Schmidl, D., Werkmeister, R. M., Lasta, M., Kaya, S., Palkovits, S., Told, R., et al., 2013, "Regulation of Optic Nerve Head Blood Flow During Combined Changes in Intraocular Pressure and Arterial Blood Pressure," J. Cereb. Blood Flow Metab., **33**(12), pp. 1850–1856.
[69] Kiyota, N., Shiga, Y., Ichinohasama, K., Yasuda, M., Aizawa, N., Omodaka, K., Honda, N., Kunikata, H., and Nakazawa, T., 2018, "The Impact of Intraocular Pressure Elevation on Optic Nerve Head and Choroidal Blood Flow," Invest. Ophthalmol. Visual Sci., **59**(8), pp. 3488–3496.
[70] Iwase, T., Akahori, T., Yamamoto, K., Ra, E., and Terasaki, H., 2018, "Evaluation of Optic Nerve Head Blood Flow in Response to Increase of Intraocular Pressure," Sci. Rep., **8**(1), p. 17235.
[71] Lu, Y., Hua, Y., Wang, B., Zhong, F., Theophanous, A., Tahir, S., Lee, P.-Y., and Sigal, I. A., 2023, "Moderately Elevated IOP May Alter Optic Nerve Head Hemodynamics Enough to Cause Mild Hypoxia Over a Substantial Part of the Lamina Cribrosa," Invest. Ophthalmol. Visual Sci., **64**(8), pp. 4732–4732.
[72] Voorhees, A., Hua, Y., Sigal, I., Roberts, C., Dupps, W., and Downs, C., 2018, "Parametric Analysis to Identify Biomechanical Risk Factors; Taking Control of Population Diversity and Experiment Variability," *Biomechanics of the Eye*, C. J. Roberts, W. J. Dupps, and C. Downs, eds., Kugler Publications, Amsterdam, The Netherlands.
[73] Hayreh, S. S., Zimmerman, M. B., Podhajsky, P., and Alward, W. L., 1994, "Nocturnal Arterial Hypotension and Its Role in Optic Nerve Head and Ocular Ischemic Disorders," Am. J. Ophthalmol., **117**(5), pp. 603–624.
[74] Graham, S. L., Drance, S. M., Wijsman, K., Douglas, G. R., and Mikelberg, F. S., 1995, "Ambulatory Blood Pressure Monitoring in Glaucoma: The Nocturnal Dip," Ophthalmology, **102**(1), pp. 61–69.
[75] Dielemans, I., Vingerling, J. R., Algra, D., Hofman, A., Grobbee, D. E., and de Jong, P. T., 1995, "Primary Open-Angle Glaucoma, Intraocular Pressure, and Systemic Blood Pressure in the General Elderly Population: The Rotterdam Study," Ophthalmology, **102**(1), pp. 54–60.
[76] Hulsman, C. A., Vingerling, J. R., Hofman, A., Witteman, J. C., and de Jong, P. T., 2007, "Blood Pressure, Arterial Stiffness, and Open-Angle Glaucoma: The Rotterdam Study," Arch. Ophthalmol., **125**(6), pp. 805–812.
[77] Bosch, A. J., Harazny, J. M., Kistner, I., Friedrich, S., Wojtkiewicz, J., and Schmieder, R. E., 2017, "Retinal Capillary Rarefaction in Patients With Untreated Mild-Moderate Hypertension," BMC Cardiovasc. Disord., **17**(1), pp. 1–11.
[78] Schiffrin, E. L., 1992, "Reactivity of Small Blood Vessels in Hypertension: Relation With Structural Changes. State of the Art Lecture," Hypertension, **19** (2_Suppl), p. II1.
[79] Muraoka, Y., Tsujikawa, A., Kumagai, K., Akiba, M., Ogino, K., Murakami, T., Akagi-Kurashige, Y., Miyamoto, K., and Yoshimura, N., 2013, "Age-and Hypertension-Dependent Changes in Retinal Vessel Diameter and Wall Thickness: An Optical Coherence Tomography Study," Am. J. Ophthalmol., **156**(4), pp. 706–714.
[80] Yu, J., Liang, Y., Thompson, S., Cull, G., and Wang, L., 2014, "Parametric Transfer Function Analysis and Modeling of Blood Flow Autoregulation in the Optic Nerve Head," Int. J. Physiol., Pathophysiol. Pharmacol., **6**(1), pp. 13–22.
[81] Mozaffarieh, M., Grieshaber, M. C., and Flammer, J., 2008, "Oxygen and Blood Flow: Players in the Pathogenesis of Glaucoma," Mol. Vision, **14**, pp. 224–233.
[82] Orgül, S., Gugleta, K., and Flammer, J., 1999, "Physiology of Perfusion as It Relates to the Optic Nerve Head," Surv. Ophthalmol., **43**, pp. S17–S26.
[83] Lu, Y., Hua, Y., Wang, B., Tian, Q., Zhong, F., Theophanous, A., Tahir, S., Lee, P.-Y., and Sigal, I. A., 2025, "Impact of Elevated IOP on Lamina Cribrosa Oxygenation: A Combined Experimental-Computational Study on Monkeys," Ophthalmol. Sci., **5**(3), p. 100725.
[84] Lu, Y., Banna, H., Yi, H., Schilpp, H., Liu, M., Zhong, F., Wang, B., et al., 2024, "Elevated IOP Reduces Lamina Cribrosa Oxygenation Both Directly Through Capillary Distortion and Indirectly by Reducing Perfusion From the Posterior Ciliary Arteries," Invest. Ophthalmol. Visual Sci., **65**(7), pp. 392–392.
[85] Lipowsky, H. H., Usami, S., and Chien, S., 1980, "In Vivo Measurements of "Apparent Viscosity" and Microvessel Hematocrit in the Mesentery of the Cat," Microvasc. Res., **19**(3), pp. 297–319.